

# Nonreciprocity of Phase Accumulation and Propagation Losses of Surface Acoustic Waves in Hybrid Magnetoelastic Heterostructures

Derek A. Bas<sup>1,\*</sup>, Roman Verba,<sup>2</sup> Piyush J. Shah,<sup>1</sup> Serhiy Leontsev,<sup>1</sup> Alexei Matyushov,<sup>3,4</sup> Michael J. Newburger,<sup>1</sup> Nian X. Sun<sup>3</sup>,<sup>5</sup> Vasyl Tyberkevich,<sup>5</sup> Andrei Slavin,<sup>5</sup> and Michael R. Page<sup>1</sup>

<sup>1</sup>Materials and Manufacturing Directorate, Air Force Research Laboratory, WPAFB, Ohio 45433, USA

<sup>2</sup>Institute of Magnetism, Kyiv, 03142, Ukraine

<sup>3</sup>Department of Electrical and Computer Engineering, Northeastern University, Boston, Massachusetts 02115, USA

<sup>4</sup>Department of Physics, Northeastern University, Boston, Massachusetts 02115, USA

<sup>5</sup>Department of Physics, Oakland University, Rochester, Michigan 48309, USA

(Received 23 June 2022; revised 19 July 2022; accepted 8 September 2022; published 3 October 2022)

Lack of nonreciprocity—in particular, nonreciprocity of phase accumulation—is one of the major drawbacks of microwave solid-state acoustic devices, which has prevented the development of acoustic isolators and circulators. Here we report the observation of the *phase* nonreciprocity of hybridized surface acoustic waves (SAWs) and spin waves in a magnetoelastic heterostructure. Our system consists of a Fe-Ga-B/Al<sub>2</sub>O<sub>3</sub>/Fe-Ga-B multilayer on top of a LiNbO<sub>3</sub> crystal. Maximum values of the observed nonreciprocal phase accumulation easily exceed  $\pi$  radians over a broad range of field conditions, which is necessary for the development of an effective circulator. In addition, under the application of bias magnetic field, the structure demonstrates tunable giant nonreciprocity of propagation losses with isolation as high as 48 dB, necessary for the development of isolators. Theoretical calculations provide an insight into the observed phenomena and demonstrate a pathway for further improvement of nonreciprocal SAW devices based on magnetoelastic coupling.

DOI: 10.1103/PhysRevApplied.18.044003

## I. INTRODUCTION

Nonreciprocity of wave propagation is a fascinating physical phenomenon, highly desirable and already widely used in microwave signal-processing techniques [1]. However, the requirement of simultaneous time- and space-reversal symmetry breaking [2–4] results in wave nonreciprocity being prohibited in the majority of simple physical systems. And while current state-of-the-art nonreciprocal devices rely on the nonreciprocity of electromagnetic waves in ferrite-based waveguides [5, 6], they are almost impossible to miniaturize below the size of several centimeters in the microwave frequency range.

A viable alternative to ferrite devices, for applications where size and weight are constrained, are microwave solid-state acoustic devices, which are well known for their excellent characteristics in the frequency band from 100 MHz to several gigahertz [7–9]. However, symmetry of fundamental laws of mechanics prohibits nonreciprocity of linear acoustic waves in solids. Inherent acoustic

nonreciprocity can be realized only in moving or rotating media [10,11], e.g., gases or liquids, and this effect is not applicable beyond the typical sound and ultrasonic frequency band. Therefore, the search for nonreciprocity in acoustic waves has prompted investigation into the interaction of elastic waves with other dynamic subsystems [12]. The idea to utilize magnetoelastic coupling for this purpose, formulated in 1972 [13], has now evolved to the theoretical prediction [14,15] and successful experimental realization [16–19] of a large nonreciprocity of propagation losses for surface acoustic waves (SAWs) in hybrid structures consisting of an acoustic (usually piezoelectric) crystal and magnetic layer or multilayer. Another type of wave nonreciprocity—nonreciprocity of the phase accumulation, required for the development of circulators—demands more care to realize using magnetoelastic coupling, and was only recently considered theoretically [20].

In this work, we study SAW propagation both theoretically and experimentally in a hybrid heterostructure consisting of Fe-Ga-B/Al<sub>2</sub>O<sub>3</sub>/Fe-Ga-B multilayer on a piezoelectric LiNbO<sub>3</sub> substrate. Here the LiNbO<sub>3</sub> provides the acoustic component and the ferromagnetic Fe<sub>71</sub>Ga<sub>17</sub>B<sub>12</sub> (Fe-Ga-B) bilayer contributes nonreciprocal

\*derek.bas.ctr@afrl.af.mil

magnetic properties, while dynamics in both materials are coupled by strong Fe-Ga-B magnetostriiction. By tuning magnetic field magnitude and direction, it becomes possible to realize sufficiently large-phase nonreciprocity and giant isolation (nonreciprocity of propagation losses), as described in Sec. II. Theoretical analysis (Sec. III) provides qualitative understanding of the measured transmission characteristics of the studied device, and also shows a pathway for the improvement of nonreciprocal characteristics, as discussed in Sec. IV.

## II. EXPERIMENTAL RESULTS

The experimental geometry and a sketch of the sample are shown in Fig. 1(a). SAWs are excited in a  $\text{LiNbO}_3$   $y$ -cut single crystal by aluminum interdigital transducers (IDTs) with a split-finger geometry, having 60 finger pairs with the minimum electrode separation of  $\lambda/8 \approx 1.5 \mu\text{m}$ . The fundamental resonance frequency of the IDTs is 287 MHz. The results below are measured at the fifth harmonic, 1435 MHz, which is chosen due to the trade-off between

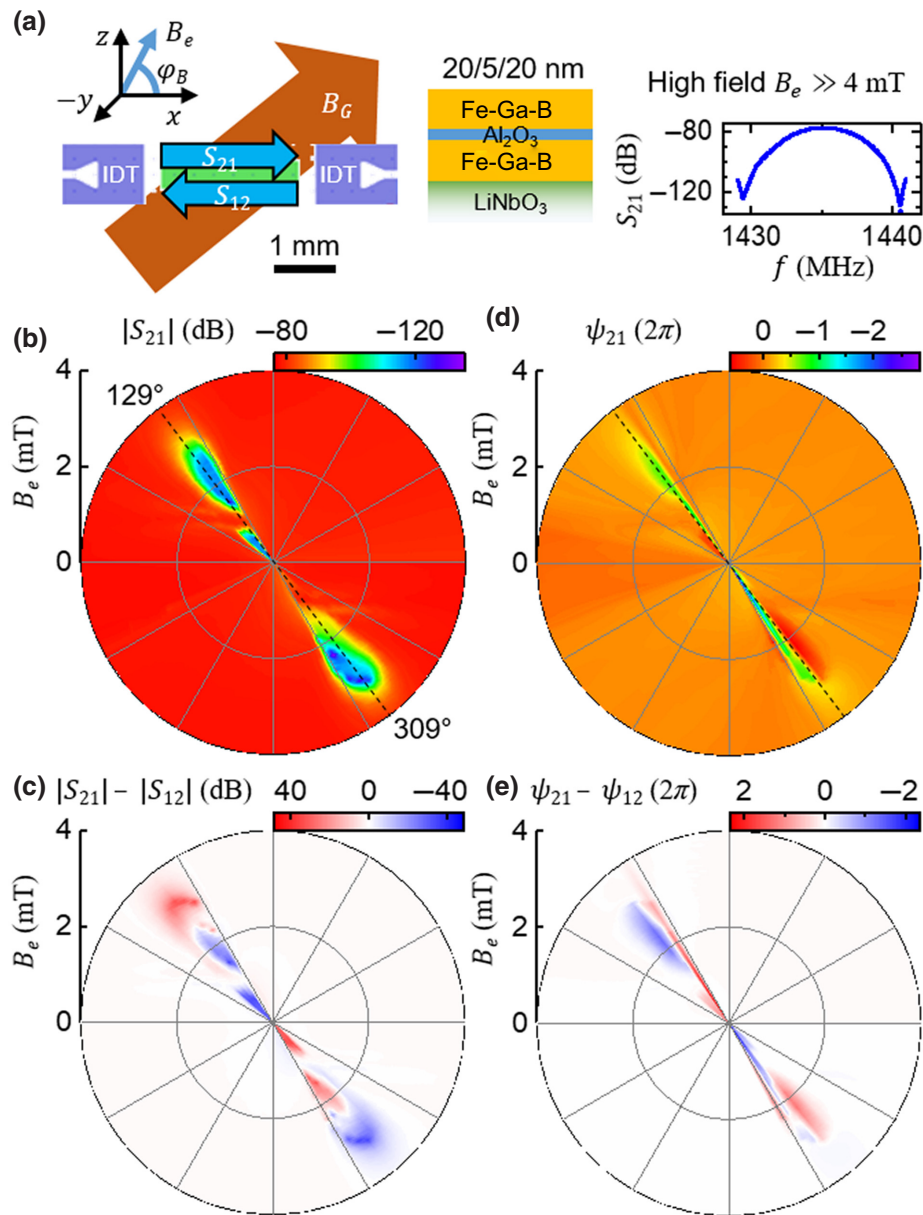


FIG. 1. (a) Left: schematic of IDTs (purple) and magnet (green), showing the *in situ* magnetic field  $B_G = 20 \text{ mT}$  applied during growth of the magnetic film and the  $S_{21}/S_{12}$  transmission coefficient, with the coordinate system. The device is nominally symmetric except for the growth field. Center: device layer schematic. Right: high-field (magnet-independent) transmission band. (b) Forward ( $S_{21}$ ) transmission magnitude as a function of applied field  $B_e$ . (c) Transmission magnitude nonreciprocity as a function of applied field  $B_e$ . (d) Forward transmission phase ( $\psi_{21}$ ). (e) Nonreciprocity of the phase accumulation.

insertion loss (which decreases at lower frequencies [21]) and the strength of magnetoelastic interaction between spin and acoustic waves (which increases at higher frequencies [14]). At this frequency, the IDT resonance has a full width at half maximum of about 3 MHz [magnet-independent transmission is shown in Fig. 1(a)]. The IDTs are wire bonded to coaxial cable adapters, connected to ports 1 and 2 of a vector network analyzer (VNA). In our measurements, the VNA simultaneously measures the magnitude and the phase of forward ( $S_{21}$ ) and reverse ( $S_{12}$ ) transmission; the phase measurement is the key aspect of the experimental part of this work.

In between the IDTs, in the propagation path of the SAWs, the Fe-Ga-B/Al<sub>2</sub>O<sub>3</sub>/Fe-Ga-B heterostructure is sputtered with the layer thicknesses 20/5/20 nm and lateral size  $L_x \times L_z = 2200 \times 500 \mu\text{m}$ . Ferromagnetic bilayers are known to demonstrate nonreciprocity of the spin-wave spectra if the static magnetizations of the layers are not parallel [22,23], which results in a much more pronounced nonreciprocity of SAW propagation, induced by magnetoelastic coupling [14,15]. During the growth of the ferromagnetic layers, a bias magnetic field  $B_G = 20 \text{ mT}$  is applied at an angle of 39° respective to the SAW propagation direction [Fig. 1(a)], which influences the direction of weak in-plane magnetic anisotropy of the Fe-Ga-B layers. During the measurements, applied magnetic field  $B_e$  is swept from 10 mT (saturated state of the bilayer) to zero at a given angle by a vector electromagnet, and the field angle  $\varphi_B$  is changed in increments of 3°.

Transmission magnitude  $|S_{21}|$ , shown in Fig. 1(b), has sharp resonances (decrease of transmission) in only two quadrants, in the vicinity of  $\varphi_B = 129^\circ$  and  $\varphi_B = 309^\circ$  applied field angles. Such a two-lobe pattern is observed in a similar bilayer system [17], while acoustic crystals interacting with a single magnetic layer more commonly display a four-lobe pattern [24]. The transmission characteristic is strongly asymmetric with respect to the origin: when either the field direction or SAW propagation direction are reversed, the transmission changes dramatically. The nonreciprocity of transmission magnitude  $|S_{21}| - |S_{12}|$  is shown in Fig. 1(c), where we see that the nonreciprocity (in other words, isolation coefficient) exceeds 40 dB at certain field angles and magnitudes. Several  $|S_{ij}|$  plots at specific field angles are shown below in Fig. 3.

During this transmission magnitude modulation, a phase-accumulation shift occurs simultaneously, and the map of these relative shifts [Fig. 1(d)] show similarity with the transmission magnitude map. There is a complex pattern of behavior between  $\varphi_B = 120^\circ$  and  $\varphi_B = 130^\circ$  (and 300°–310°), where the phase shifts between opposite traveling SAWs can differ by over two full cycles ( $4\pi$  radians). The degree of this phase nonreciprocity is shown in Fig. 1(e). It is worth noting that the phase nonreciprocity and magnitude nonreciprocity patterns are not identical, and there are regions showing strong phase nonreciprocity

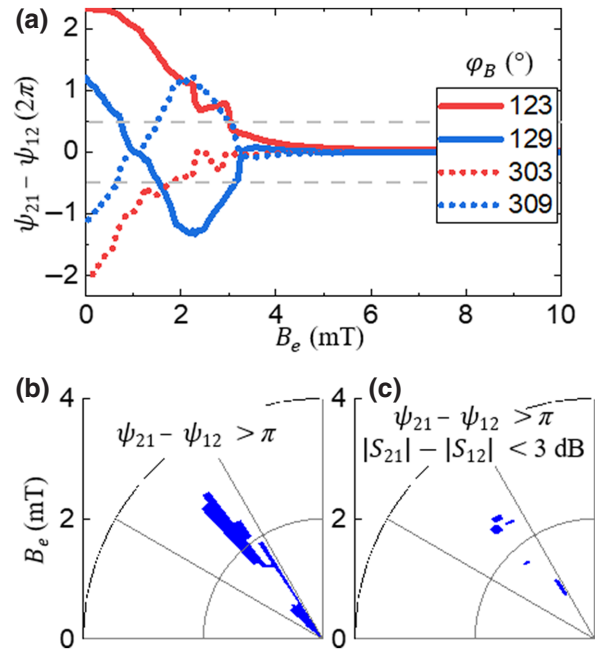


FIG. 2. Phase nonreciprocity. (a) Measured nonreciprocal phase accumulation for different applied field angles. Dashed gray lines indicate  $\pi$  phase nonreciprocity, which is the necessary condition for phase device applications. (b) Map of the field conditions for which the phase nonreciprocity is sufficient,  $|\psi_{21} - \psi_{12}| \geq \pi$ . (c) Intersection of phase nonreciprocity map and weak magnitude reciprocity (where the difference in absorption is less than 3 dB).

and weak magnitude nonreciprocity and vice versa, which is useful for certain applications.

Several line cuts of the phase nonreciprocity pattern are shown in Fig. 2(a). Depending on the applied field angle  $\varphi_B$ , the field dependence of the phase accumulation nonreciprocity ( $\psi_{21} - \psi_{12}$ ) can be almost monotonic or acquire a complex nonmonotonic shape. The theory section below explains this complexity in the field dependence of phase nonreciprocity, as well as of magnitude nonreciprocity. From the perspective of applications, this can be quite a useful feature, as it allows for a simple reconfiguration of a device functionality by varying the field magnitude by just several tenths of millitesla, suggesting that the studied structure is a promising, highly versatile rf tool.

For the development of a circulator, the necessary condition of the phase nonreciprocity is the accumulation of  $\pi$ -phase difference between counterpropagating waves,  $|\psi_{21} - \psi_{12}| = \pi$  [20]. From Fig. 2(a), one finds that in our device this condition is well exceeded over a broad range of field conditions. Moreover, the phase accumulation is length dependent, so the 2.2-mm-long magnet could be miniaturized even further while preserving the functionality. The whole region where  $|\psi_{21} - \psi_{12}| \geq \pi$  is highlighted in the field-angle diagram shown in Fig. 2(b).

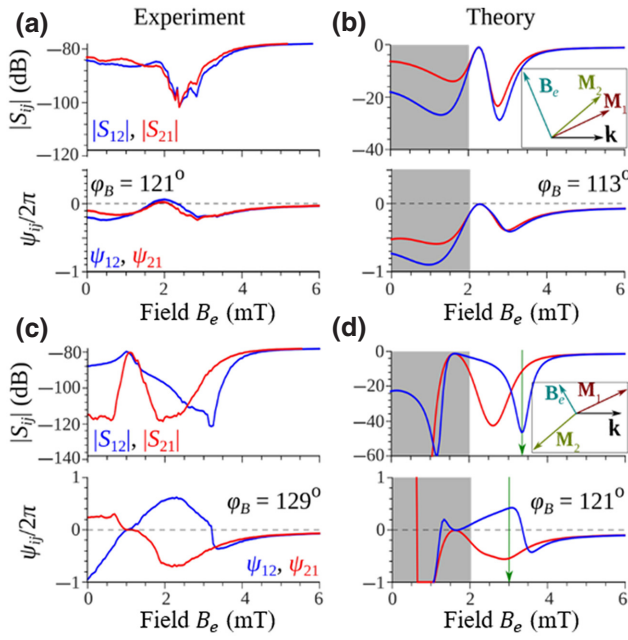


FIG. 3. Experimental (a),(c) and calculated (b),(d) magnitude  $|S_{ij}|$  and phase  $\psi_{ij}$  of the SAW transmission for different angles of the applied bias magnetic field. Theoretical plot (b) corresponds to a *quasiferromagnetic* state of the bilayer, while plot (d) corresponds to the *quasiantiferromagnetic* state. Directions of the applied field  $\mathbf{B}_e$ , SAW wave vector  $\mathbf{k}$ , and static magnetizations  $\mathbf{M}_i$  of the layers at a vanishing bias field are shown in the insets. The gray shaded area in (b),(d) corresponds to a bias field magnitude that is smaller than the mean anisotropy field, at which a *nonuniform* magnetic state is expected. Green arrows in the frame (d) show the points of large isolation (top panel) and large phase nonreciprocity (bottom panel). Spin-wave spectra for these cases are presented in Fig. 4.

We demonstrate that a single magnetoelastic device structure can act as both an isolator with extremely high contrast ( $>48$  dB) and a nonreciprocal phase shifter. However, if a purely “phase-based” device is desired, as in the example of the circulator proposed in Ref. [20], it may be detrimental to have simultaneous nonreciprocity in propagation losses. Therefore, in Fig. 2(c), we highlight the field conditions for which the nonreciprocity of losses is weak,  $|S_{21} - S_{12}| < 3$  dB, while the phase nonreciprocity is sufficient,  $|\psi_{21} - \psi_{12}| \geq \pi$ . Although our device demonstrates a rather small region where both conditions are satisfied, it is an experimental demonstration of an almost equal loss and sufficiently high-phase nonreciprocity of SAWs induced by magnetoelastic coupling. The possible directions for the improvement of the “phase nonreciprocity functionality” are discussed below.

### III. THEORY

To gain a deeper understanding of the experimental results, we perform theoretical calculations of the

transmission characteristics of the studied heterostructure. A general approach for the calculation of characteristics (damping rate and frequency) of coupled magnetoelastic waves in heterostructures and transmission characteristics of devices based on them is described in Ref. [14]. Overall, these characteristics are determined by many material parameters, some of which are not known precisely, especially for nanoscale-thick layers. Two main factors affecting the coupled waves are (i) dispersion relations of the hybridized SAW and spin wave (SW) determining the frequency distance between the pure acoustic and pure spin waves, and (ii) the angle  $\varphi_M$  between the SAW and SW propagation direction and the direction of static magnetization of the structure. In the case of thin magnetic layers, the magnetoelastic coupling demonstrates  $|\sin(2\varphi_M)|$  dependence [14,24].

These quantities can be measured directly or extracted from other measurements with reasonably high precision. However, the strength of the coupling between SAWs and SWs also depends on the magnetoelastic tensor of a ferromagnet (the magnitude and even symmetry of which can differ in thin layers from reference values measured for bulk samples) and on the structure (profile) of acoustic waves in ferromagnetic layers. These profiles are especially hard to determine because the SAW profile depends on the mechanical properties of thin ferromagnetic layers and the properties of the contact between the ferromagnetic layer and the adjacent piezoelectric crystal. In the case of simple heterostructures having a single ferromagnetic layer, the mentioned factors mainly affect the strength of the resulting coupling of acoustic and spin waves, almost preserving the structure of the coupling dependence on external parameters (e.g., field, frequency, etc.). The case of ferromagnetic bilayers is much more complex, because contributions from the layers can enhance or compensate each other [15], and thus can lead to the appearance of a *fine structure* of the coupling.

The theory of SW spectrum in an antiferromagnetically ordered magnetic bilayer was developed in Refs. [14,15]. These results demonstrate a strong nonreciprocity of this spectrum, dependent on the direction of the wave propagation with respect to the direction of the magnetization in magnetic layers [see e.g., Eq. (A1) in Ref. [15]]. In the case when the in-plane bias magnetic field is applied, the spectrum of hybridized SAW and SW waves becomes even more complex, as the variation in the direction and magnitude of the bias magnetic field will lead to the variation in the relative orientations of the static magnetizations in magnetic layers, and, therefore, to the variation of the degree of nonreciprocity of waves propagating in the opposite in-plane directions. This property of the hybridized SAW and SW spectrum in the layered heterostructure, shown in Fig. 1(a), is further illustrated in Fig. 4, where the optimum conditions for phase [Fig. 4(a)] and amplitude [Fig. 4(b)] nonreciprocity are found numerically.

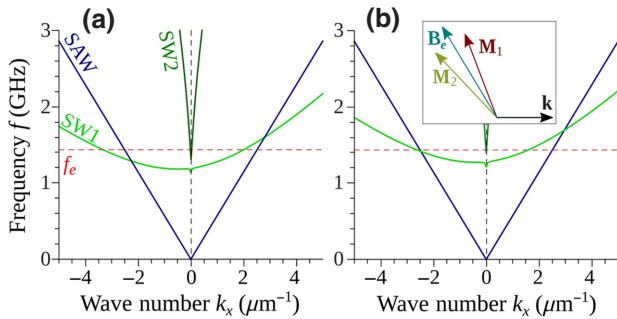


FIG. 4. Calculated spectra of SAW and spin waves in a quasiantiferromagnetic state for large phase nonreciprocity (a) and large isolation (b). The bias magnetic field is applied at the angle  $\varphi_B = 121^\circ$  and its magnitude is  $B_e = 3.05$  mT in (a) and  $B_e = 3.35$  mT in (b). The spin-wave spectrum consists of two branches, SW1 and SW2, the latter of which is higher in frequency, and does not contribute to the magnetoelastic coupling with SAWs at the studied frequency. Mode repulsion of hybridized magnetoelastic waves at the crossing points is on the order of 20 MHz, and is not visible on this frequency scale. The excitation frequency  $f_e = 1435$  MHz is marked by a dashed horizontal line. The inset in frame (b) shows the directions of the static magnetizations of the layers, applied field, and SAW wave vector at  $B_e = 3.35$  mT.

Due to the above-mentioned reasons, here we are not trying to reproduce quantitatively all the results by fitting many unknown parameters, but instead, make calculations in a simplified model using measured and literature material parameters. The magnetic layers are characterized by the saturation magnetization  $\mu_0 M_s = 1.2$  T, in-plane anisotropy with the effective field  $B_{\text{an},1} = 2.4$  mT and  $B_{\text{an},2} = 1.9$  mT and hard axis directed at  $\varphi_{\text{an},1} = 115^\circ$  and  $\varphi_{\text{an},2} = 130^\circ$  respective to SAW propagation direction, and Gilbert damping  $\alpha_G = 0.0045$ , as are extracted from ferromagnetic resonance measurements (see details in Appendix A). Literature values of exchange length  $\lambda_{\text{ex}} = 4.7$  nm and magnetoelastic constants  $B_1 = B_2 = 9.38$  MJ/m<sup>3</sup> are used [17]. For elastic parameters of LiNbO<sub>3</sub>, we use longitudinal and transversal sound velocities  $c_l = 6700$  m/s and  $c_t = 3780$  m/s [21,25], which gives SAW velocity  $c_{\text{SAW}} = 3488$  m/s, along with the density  $\rho = 4650$  kg/m<sup>3</sup>. In our calculations, we assume that the spatial structure of a SAW in a magnetic layered structure is the same as it would have been in a simple LiNbO<sub>3</sub> crystal (which is a good approximation for magnetic layers that are thin compared to the SAW penetration depth and assuming a good mechanical contact between all the layers). Finally, very narrow frequency width of the IDT resonance [Fig. 1(a)] allows us to eliminate all the nonresonant excitation effects [14], and to calculate all the parameters locally, at the IDT resonance wave number. Therefore, propagation losses are calculated simply as  $|S_{ij}| = -20 \log[\Gamma_{\text{me}} L_x / c_{\text{SAW}}]$  and the phase accumulation is approximated as  $\psi_{ij} = (\omega_{\text{me}} - \omega_{\text{SAW}}) L_x / c_{\text{SAW}}$ , with  $\Gamma_{\text{me}}$

and  $\omega_{\text{me}}$  being the damping rate and frequency of a coupled SAW and SW.

In our sample, ferromagnetic layers possess slightly different directions of the anisotropy axes. Therefore, depending on the direction of the applied bias field we expect the formation of different relative magnetization states (it is assumed that the indirect exchange interaction is absent, and that the dipolar interaction does not affect the mutual orientation of the static magnetizations of the layers). For the majority of the magnetization angles, the projections of the bias field onto the anisotropy axes of the magnetic layers are co-directed, and when the field is reduced from high to low the formation of a quasiferromagnetic state is expected.

Such a structure of magnetization in a small bias field applied at the angle  $\varphi_B = 113^\circ$  to the SAW propagation direction is shown in the inset of Fig. 3(b), which gives an example of the transmission characteristic in such a state. It is very similar to the magnetization structure in our experimental multilayer measured at a somewhat different applied field angle ( $8^\circ$  larger). The difference in angle is attributed to the above-mentioned model simplifications and the fine structure of the magnetoelastic coupling.

In our calculations, pure SAWs exhibit negligible losses ( $-1$  dB [26]), which correspond to the experimental value of about  $-79$  dB, determined by the losses in the IDTs and by the impedance mismatch with the microwave supply line. In this case, the spin-wave spectrum is almost reciprocal, and transmission minima at about 3 mT for positive and negative propagation directions are almost the same. The observed weak nonreciprocity is a result of a weak contribution coming from the shear strain  $u_{xz}$  [16].

At larger applied fields, above 4 mT, the effect of magnetoelastic coupling on the SAW transmission vanishes, simply because the spin-wave spectra are shifted to higher frequencies, and do not intersect the SAW spectrum in the vicinity of the excitation frequency  $f_e = 1435$  MHz. High transmission at about 2.25 mT is related to the fact that the static magnetizations of the layers become almost perpendicular to the propagation direction, resulting in a vanishing magnetoelastic coupling.

At low field (below 2 mT) we see a significant quantitative difference from the high-field case. The experimental curves still show some nonreciprocity, but the theoretical values of nonreciprocity are much larger. In this case, the observed values of the nonreciprocity are determined by the nonreciprocity of spin-wave spectra appearing due to the noncollinear magnetic state of the magnetic layers. At these relatively small bias fields, which are smaller than the anisotropy fields, the magnetic state of the magnetic layers is expected to be nonuniform, and magnetic domains are expected to be formed [as confirmed by magneto-optic Kerr effect (MOKE) measurements in Appendix A], which is not accounted for in our calculations. Therefore, in a real sample, some domains could give vanishing contributions

to the coupling, some domains could have contributions of the opposite sign, and, thus, the overall magnetoelastic coupling effect becomes weaker (the domain magnetization direction could be significantly different from the direction expected in a uniform magnetic state at the same bias field).

When the field is directed in between the hard axes of the layers, the formation of a quasiantiferromagnetic state is expected, which relaxes to the oppositely directed magnetization state when the field is reduced to zero. This state is shown in the inset of Fig. 3(d). In such a case, the spin-wave spectrum is sufficiently nonreciprocal even at moderate bias fields, leading to the different positions of the transmission minima for opposite propagation directions, and consequently, to the large nonreciprocity of the SAW losses [Fig. 4(d)]. The phase nonreciprocity is also pronounced, especially in between the transmission minima.

We would like to note a good qualitative and quantitative similarity between the theoretical and experimental results at the magnetization angles that are only slightly different. At the small bias fields, we observe the same feature as in the ferromagnetic state. Qualitatively, the dependence is similar: in particular, the sign of phase and amplitude nonreciprocity is the same as in the experiment, but calculated nonreciprocity values are much larger. For example, calculations give the minimum transmission of  $|S_{21}| < -650$  dB, maximum isolation  $|S_{21} - S_{12}| > 600$  dB, and phase nonreciprocity up to  $\psi_{21} - \psi_{12} \approx 22\pi$ . The main reason for this discrepancy between the experiment and the results of our simplified model is the existence of the above-mentioned nonuniform magnetic state of the system at low bias fields. There is, however, another possible reason limiting the magnitude of the maximal isolation, discussed in the next section.

The calculated spectra of the spin and acoustic waves at the field values corresponding to the maximal phase nonreciprocity and isolation (except for the small-field range, shown by gray shading in Fig. 3) are shown in Fig. 4. The large isolation, as expected, is achieved when the spin-wave dispersion curve crosses the SAW dispersion curve at the working frequency for one propagation direction only, as shown in Fig. 4(b). In contrast, the large phase nonreciprocity is observed when the working frequency is situated between the crossing points of dispersion curves for the opposite propagation directions [Fig. 4(a)]. This, also, leads to the *almost equal* values of the propagation losses in two opposite propagation directions,  $|S_{21}| \approx |S_{12}|$  (i.e., to the practical absence of the amplitude nonreciprocity).

It is worthwhile to note that the magnetoelastic coupling between the spin and acoustic waves in the studied case is not large—the width of the magnetoelastic band gaps is about 20 MHz, which is significantly smaller than the frequency distance from a band gap to the working frequency. In the scale of Fig. 4 these band gaps, as well as the

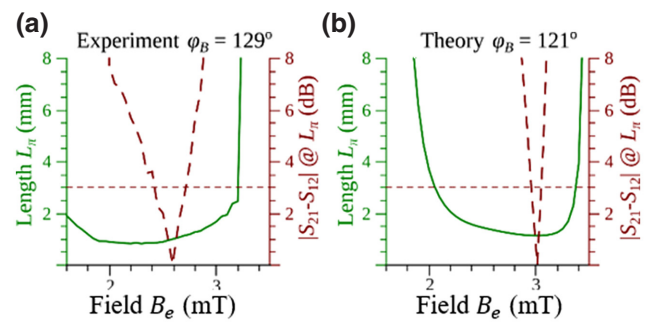


FIG. 5. Propagation length  $L_\pi$  corresponding to nonreciprocal phase shift  $|\psi_{21} - \psi_{12}| = \pi$  (left axis, solid line), and nonreciprocity of losses  $|S_{21} - S_{12}|$  at the propagation length  $L_\pi$  (right axis, dashed line) as functions of the magnitude of the bias applied field  $B_e$ , calculated from experimental data for  $\varphi_B = 129^\circ$  (a) and theoretical data for  $\varphi_B = 121^\circ$  (b). The horizontal dashed line in both frames corresponds to the nonreciprocity of losses equal to 3 dB.

modification of the SAW spectrum due to the magnetoelastic coupling, would not be visible. Therefore, our experiment confirms the idea [20] that the phase nonreciprocity of a magnitude sufficient for practical applications (e.g., design of effective circulators) could be achieved when working at the sides of the magnetoelastic band gaps where the insertion losses are relatively weak, and almost equal in both propagation directions.

To demonstrate explicitly that the development of practical SAW and SW circulators, when working at the sides of the magnetoelastic band gaps, is realistic, we present in Fig. 5 dependences of the propagation length  $L_\pi$ , corresponding to the nonreciprocal phase shift  $|\psi_{21} - \psi_{12}| = \pi$  (left axis, solid line), and the nonreciprocity of losses  $|S_{21} - S_{12}|$  at the propagation length  $L_\pi$  (right axis, dashed line) on the magnitude of the bias applied field  $B_e$ . These dependencies are calculated from experimental (a) and theoretical (b) data as  $L_\pi = L_x \pi / |\psi_{21}(L_x) - \psi_{12}(L_x)|$  and  $S_{ij}(L_\pi) = S_{ij}(L_x) L_\pi / L_x$ , where  $S_{ij}(L_x)$  and  $\psi_{ij}(L_x)$  are transmission magnitude and phase at the experimental sample length  $L_x = 2.2$  mm. It is clear from Fig. 5, that both in theory and experiment the wave-propagation length necessary to achieve the nonreciprocal phase shift of  $\pi$ , needed for the operation of a circulator [20], does not exceed  $L_\pi < 1-2$  mm in a wide range of bias magnetic fields. Although the bias-field interval where the nonreciprocity of losses  $|S_{21} - S_{12}|$  at  $L_\pi$  does not exceed 3 dB is much narrower [in the experiment it is about 0.3 mT around the bias field of  $B_e = 2.6$  mT, see Fig. 5(a) and see also Fig. 2(c)], it is still sufficient for the development of a practical SAW and SW circulator.

#### IV. DISCUSSION

In this section, we discuss the limitations of our samples and formulate the possibilities for the

improvement of working characteristics of nonreciprocal SAW devices (e.g., wave isolators) based on the SAW and SW magnetoelastic interaction. As is clear from the above-presented materials, our experimental device already demonstrates a large isolation magnitude (of up to 48 dB), which meets or exceeds the isolation in the state-of-the-art commercial ferrite isolators [27].

At the same time, it may be desirable to reduce the device sizes (note that transmission modulation characteristics, including isolation, scale linearly with the device length) or to further enhance the isolation magnitude. In our experiment, we find almost the same minimum value of transmission, about  $-120$  dB, for different values and directions of the applied magnetic field (the noise floor of the measurement is below  $-130$  dB). In particular, it is clearly seen in the dependence shown in Fig. 3(c) that the bias-field dependence of  $|S_{21}|$  is almost flat at the minimum transmission level. Such flat dependence is hard to explain, as the frequency distance between the SW and SAW dispersion curves varies significantly with the bias field. In addition, in the low-field region, theory predicts much smaller transmission (i.e., the much stronger effect of the magnetoelastic coupling).

These facts force us to conclude that the minimal transmission level is determined by transmission channels unrelated to the magnetoelastic interaction. These could be contributions of the other acoustic modes, e.g., thickness or longitudinal modes, which are much less sensitive to the surface magnetic layer, or by SAWs propagating sideways in the magnetic layer. Therefore, if it is desirable to further enhance isolation, the optimization of characteristics of the acoustic system itself may be more useful than the optimization of the magnetoelastic coupling.

Regarding the *phase* nonreciprocity, we point out above that our sample demonstrates sufficient nonreciprocity of the phase accumulation (which exceeds  $\pi$  radians) to support the practical design of acoustic circulators. Also, note that the propagation losses at the points of high phase nonreciprocity are quite significant, see Figs. 3(c) and 3(d). It was theoretically shown [20] that the propagation loss in a  $\pi$ -phase nonreciprocal shifter is determined by the relation of the nonreciprocal splitting of spin-wave dispersion  $\Delta\omega_{nr}$  (frequency distance between the SAW and SW dispersion crossing points for opposite propagation direction), strength of the magnetoelastic coupling between spin and acoustic waves, characterized by the width of the magnetoelastic band gaps  $\Delta\omega_{me}$ , and damping rates of SAWs and spin waves  $\Gamma_{SAW}$  and  $\Gamma_{SW}$ . The optimal case of sufficient phase nonreciprocity and low propagation losses is achieved when the conditions  $\Delta\omega_{nr} \gg \Delta\omega_{me} \gg \sqrt{\Gamma_{SAW}\Gamma_{SW}}$  and  $\Delta\omega_{me} \geq \Gamma_{SW}$  are satisfied. In our case, for the field  $B_e = 3.05$  mT [dispersions are shown in Fig. 4(a)], we get  $\Delta\omega_{nr}/2\pi = 218$  MHz,  $\Delta\omega_{me}/2\pi \approx 12$  MHz,  $\Gamma_{SAW}/2\pi = 30$  kHz, and  $\Gamma_{SW}/2\pi \approx 90$  MHz. Thus, the first condition is satisfied, while the second ( $\Delta\omega_{me} \geq \Gamma_{SW}$ )

is not. Relatively large spin-wave damping despite relatively small Gilbert constant ( $\alpha_G = 0.0045$ ) is related to the large precession ellipticity (the ellipticity-related factor is  $\varepsilon \approx 12$  [28]) and it affects the SW damping rate as  $\Gamma_{SW} = \alpha_G \varepsilon \omega_{SW}$ . The large values of the precession ellipticity are common for thin magnetic films in low bias magnetic fields and small wave numbers of SW modes.

At a larger working frequency (e.g., several gigahertz), at least one of the above-mentioned factors becomes unimportant, and one should expect a significantly better transmission in a phase-nonreciprocal SAW device. For lower frequencies, on the order of 1 GHz, a viable alternative could be the utilization of ferromagnetic materials with certain perpendicular anisotropy, which partially (but not fully) compensates demagnetization fields and makes SW precession less elliptical.

Finally, we would like to point out that a better nonreciprocity of SAW and SW propagation is expected in low or even zero magnetic bias fields. Indeed, if the static magnetizations of the magnetic layers are aligned almost antiferromagnetically, the nonreciprocity of the spin-wave spectrum is maximal [22,23]. However, in our samples nonuniform magnetization hinders utilization of all the benefits in this range of bias fields. An evident solution is the usage of ferromagnetic bilayers with antiferromagnetic interlayer interaction (Ruderman-Kittel-Kasuya-Yosida interaction via a properly thin spacer). These systems, often called synthetic antiferromagnets, demonstrate nice antiferromagnetic alignment in zero field independently of the field sweep direction, in contrast with simple bilayers without interlayer exchange coupling. Also, note that in the case of uncoupled magnetic layers with the same direction of the anisotropy easy axes, achievement of antiferromagnetic alignment would be even harder than in the studied case of magnetic layers having anisotropy axes of slightly different directions. This method of utilization of synthetic antiferromagnetics has been successfully realized in a very recent work [29], and has indeed shown larger magnitude nonreciprocity per unit length.

## V. CONCLUSION

In conclusion, we experimentally demonstrate nonreciprocity of propagation losses and phase accumulation of hybridized SAW and SW in a magnetoelastic layered heterostructure Fe-Ga-B/Al<sub>2</sub>O<sub>3</sub>/Fe-Ga-B on LiNbO<sub>3</sub>. Depending on the strength and direction of bias magnetic field, our device based on this heterostructure demonstrates nonreciprocity of the phase accumulation exceeding  $\pi$  radians several times, which is sufficient for practical applications in SAW circulators, as well as giant nonreciprocity of propagation losses with isolation as high as 48 dB. Our approximate theoretical model of wave hybridization and propagation in this heterostructure reveals that both large nonreciprocal losses and large

phase nonreciprocity are achieved in a quasiantiferromagnetic state of the magnetic layers in the heterostructure. The first effect manifests itself when the SW dispersion curve crosses the SAW dispersion curve at the working frequency for one propagation direction only, while the second effect takes place when the working frequency is situated between the magnetoelastic hybridization points for the opposite propagation directions.

In our opinion, the promising directions for the further improvement of characteristics of the nonreciprocal SAW and SW devices are related to the possible utilization of synthetic antiferromagnets, use of higher working frequencies and/or use of ferromagnetic materials with partially compensated in-plane shape anisotropy, as well as suppression of parasitic acoustic transmission channels.

## ACKNOWLEDGMENTS

This work is partially supported by the Air Force Office of Scientific Research (AFOSR) Award No. FA955020RXCOR074, by the Air Force Office of Scientific Research under the MURI Grant No. FA9550-19-1-0307, by the DARPA TWEED Grant No. DARPA-PA-19-04-05FP-001, by Ministry of Education and Science of Ukraine under the Project No. 0121U110107, and by the Oakland University Foundation.

## APPENDIX A: SUPPLEMENTAL MEASUREMENTS

### Ferromagnetic resonance

To determine the nature of the magnetic film, ferromagnetic resonance ( $S_{\text{FMR}}$ ) is measured over the 1–35 GHz frequency range. The wire bonds are removed and the whole device is placed upside down with the magnet in contact with a coplanar waveguide (CPW), which drives the microwaves. A rotation series is completed with the magnet oriented both parallel and perpendicular to the CPW, with the orientation of the static field adjusted from  $-45^\circ$  to  $+45^\circ$  relative to the CPW, to complete a  $180^\circ$  rotation in the sample plane in increments of  $5^\circ$ . The result at 1435 MHz (Fig. 6) displays a similar pattern to the result of acoustically driven spin-wave resonance at the same frequency, except with two distinct lobes slightly displaced, one for each of the Fe-Ga-B layers. At 4 GHz [Fig. 6(b)] we fit the resonance to two sine waves, giving the angles at which resonant field  $B_0$  occur to be  $115$  and  $130^\circ$ . The anisotropy fields of the layers, defined as the amplitude of each sine wave, are  $B_{\text{an}} = 2.4$  and  $1.9$  mT, which we use in the Kittel fit below to determine the magnetic constants.

The frequency dependence is shown in Fig. 6(c) where we can see the two distinct resonances. These are modeled

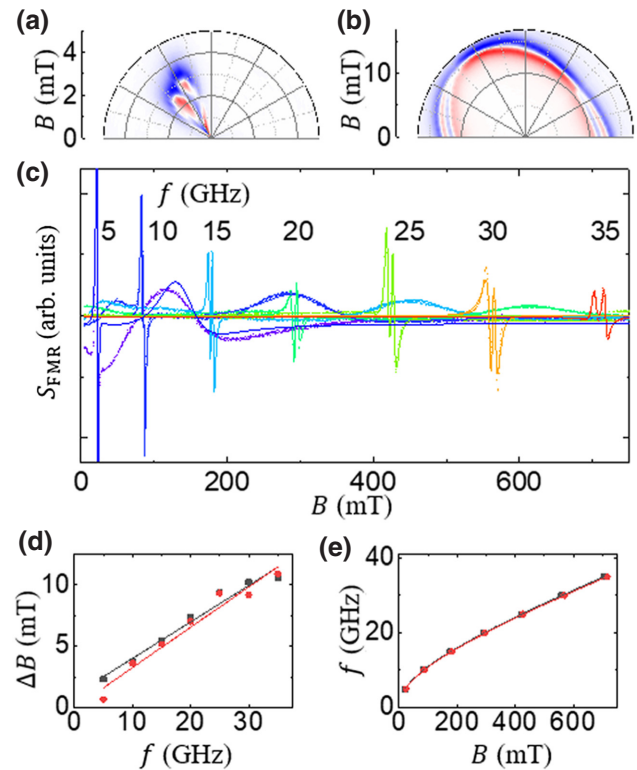


FIG. 6. FMR results on the Fe-Ga-B heterostructure. Rotation dependence at 1.435(a) and 4 GHz (b). (c) Frequency sweep. Each curve is fitted with a double Lorentzian derivative giving two positions  $B_0$  and linewidths  $\Delta B$ . (d) Linear fits (solid line) of the FMR linewidths at the lower (black) and higher (red) field resonances. (e) Kittel fits of the FMR resonance frequencies for the lower (black) and higher (red) field resonances.

by a double Lorentzian derivative:

$$S_{\text{FMR}} = y_0 + \frac{4k_1\Delta B(B - B_0)}{[4(B - B_0)^2 + \Delta B^2]^2} - \frac{k_2[\Delta B^2 - 4(B - B_0)^2]}{[4(B - B_0)^2 + \Delta B^2]^2} + \frac{4k_3\Delta B(B - B_0)}{[4(B - B_0)^2 + \Delta B^2]^2} - \frac{k_4[\Delta B^2 - 4(B - B_0)^2]}{[4(B - B_0)^2 + \Delta B^2]^2} \quad (\text{A1})$$

From the fits we obtain a resonance field  $B_0$  and a linewidth  $\Delta B$  for each individual layer. Figures 6(d) and 6(e) show the fits for the extracted parameters. The linear fit for the linewidth is  $\Delta B = \Delta B_0 + (4\pi\alpha/\gamma)f$ , and the Kittel fit is  $f = (\gamma/2\pi)\sqrt{(B + B_{\text{an}})(B + B_{\text{an}} + \mu_0M_s)}$ . From this we obtain for the lower- and higher-field resonances  $\Delta B_0 = 1, 0$  mT,  $\mu_0M_s = 1.2, 1.2$  T,  $\gamma/2\pi = 0.03, 0.03$  GHz/mT,  $\alpha = 0.0045, 0.0050$ . These magnetic parameters match

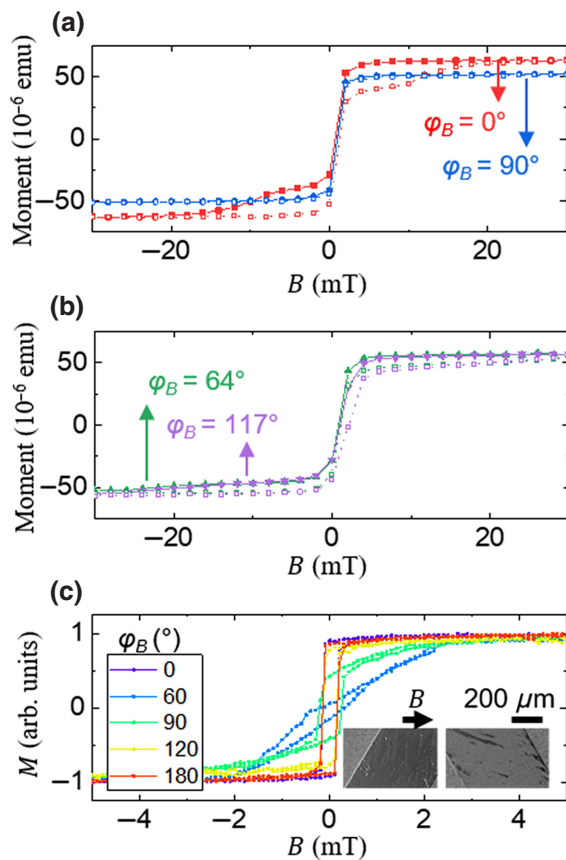


FIG. 7. Hysteresis loops from the Fe-Ga-B heterostructure. (a) Loops measured via VSM for field parallel and perpendicular to SAW  $k$  vector. (b) Loops measured via VSM for field at  $64^\circ$  and  $117^\circ$  relative to the SAW  $k$  vector. High (+) to low (−) sweeps indicated by solid markers and solid lines, and − to + indicated by empty markers and dotted lines. (c) Hysteresis loops measured via MOKE at varying angles. Left (right) inset shows horizontal  $B$  field with sample rotated to  $60^\circ$  ( $120^\circ$ ).

those previously measured for this heterostructure with 18% boron content [30].

### Vibrating sample magnetometry and magneto-optic Kerr effect microscopy

Quasistatic dc magnetic properties are measured using a Quantum Design cryogen-free Physical Property Measurement System instrument with a vibrating sample magnetometry (VSM) attachment unit. Room-temperature magnetic hysteresis loops are collected in the range  $\pm 40$  mT using sufficiently small step size to capture both sample saturation and coercive field. Substrates containing Fe-Ga-B structures are hand cut to less than 4-mm-wide pieces and mounted on quartz sample holders with VGE varnish to minimize any magnetic background. To analyze anisotropy effects each sample is measured at different orientations with respect to the applied magnetic field by slightly rotating the substrates during mounting.

The red curve in Fig. 7(a) shows that when the field is parallel to the SAW travel axis, there is a single magnetization reversal at 0 field affecting the majority of the spins to magnetize the structure to about half of  $M_s$  in the opposite direction. This is followed by a gradual switching of domains until the entire sample is saturated. In contrast, when the field is applied along the width of the magnet, there is a much simpler hysteresis loop with only a single switching event. The gradual domain switching becomes slower until a maximum at about  $60$  or  $120^\circ$  [Fig. 7(b)], where it takes the greatest magnitude of field reversal to fully saturate.

The VSM is sensitive to the entire volume of the magnetic sample. In contrast, MOKE measurements are surface sensitive, giving hysteresis of only the top layer. In Fig. 7(c) we see that the top layer behaves very differently at  $60$  and  $120^\circ$ , in opposition to the corresponding VSM measurement. The insets show the field applied along the horizontal axis with the sample at  $60$  and  $120^\circ$ , and in both cases the domains tend to align in the same direction, corresponding to the direction of the growth field. From this it becomes evident that the gradual change in magnetization seen in the VSM and MOKE loops seems to be from a domain-pinning phenomenon present in each of the two ferromagnetic layers.

- [1] A. Kord, D. L. Sounas, and A. Alù, Microwave nonreciprocity, *Proc. IEEE* **108**, 1728 (2020).
- [2] M. Tanter, J.-L. Thomas, F. Coulouvrat, and M. Fink, Breaking of time reversal invariance in nonlinear acoustics, *Phys. Rev. E* **64**, 016602 (2001).
- [3] F. D. M. Haldane and S. Raghu, Possible Realization of Directional Optical Waveguides in Photonic Crystals with Broken Time-Reversal Symmetry, *Phys. Rev. Lett.* **100**, 013904 (2008).
- [4] Z. Wang, Y. D. Chong, J. D. Joannopoulos, and M. Soljacic, Reflection-Free One-Way Edge Modes in a Gyromagnetic Photonic Crystal, *Phys. Rev. Lett.* **100**, 013905 (2008).
- [5] A. G. Gurevich and G. A. Melkov, *Magnetization Oscillations and Waves* (CRC Press, New York, 1996).
- [6] B. K. Kuanr, V. Veerakumar, R. Marson, S. R. Mishra, R. E. Camley, and Z. Celinski, Nonreciprocal microwave devices based on magnetic nanowires, *Appl. Phys. Lett.* **94**, 202505 (2009).
- [7] C. Campbell, *Surface Acoustic Wave Devices and Their Signal Processing Applications* (Academic Press, Saint Louis, 1989).
- [8] D. Morgan, in *Surface Acoustic Wave Filters: With Applications to Electronic Communications and Signal Processing (Studies in Electrical and Electronic Engineering)*, 2nd ed. (Academic Press, London, 2010).
- [9] P. Delsing, A. N. Cleland, M. J. A. Schuetz, J. Knörzer, G. Giedke, J. I. Cirac, K. Srinivasan, M. Wu, and K. C. Balram, The 2019 surface acoustic waves roadmap, *J. Phys. D: Appl. Phys.* **52**, 353001 (2019).

- [10] R. Fleury, D. L. Sounas, C. F. Sieck, M. R. Haberman, and A. Alù, Sound isolation and giant linear nonreciprocity in a compact acoustic circulator, *Science* **343**, 516 (2014).
- [11] C. P. Wiederhold, D. L. Sounas, and A. Alù, Nonreciprocal acoustic propagation and leaky-wave radiation in a waveguide with flow, *J. Acoust. Soc. Am.* **146**, 802 (2019).
- [12] J. Heil, B. Lüthi, and P. Thalmeier, Nonreciprocal surface-acoustic-wave propagation in aluminum, *Phys. Rev. B* **25**, 6515 (1982).
- [13] M. F. Lewis and E. Patterson, Acoustic-surface-wave isolator, *Appl. Phys. Lett.* **20**, 276 (1972).
- [14] R. Verba, I. Lisenkov, I. Krivorotov, V. Tiberkevich, and A. Slavin, Nonreciprocal Surface Acoustic Waves in Multilayers with Magnetoelastic and Interfacial Dzyaloshinskii-Moriya Interactions, *Phys. Rev. Appl.* **9**, 064014 (2018).
- [15] R. Verba, V. Tiberkevich, and A. Slavin, Wide-Band Nonreciprocity of Surface Acoustic Waves Induced by Magnetoelastic Coupling with a Synthetic Antiferromagnet, *Phys. Rev. Appl.* **12**, 054061 (2019).
- [16] R. Sasaki, Y. Nii, Y. Iguchi, and Y. Onose, Nonreciprocal propagation of surface acoustic wave in Ni/LiNbO<sub>3</sub>, *Phys. Rev. B* **95**, 020407(R) (2017).
- [17] P. J. Shah, D. A. Bas, I. Lisenkov, A. Matyushov, N. X. Sun, and M. R. Page, Giant nonreciprocity of surface acoustic waves enabled by the magnetoelastic interaction, *Sci. Adv.* **6**, eabc5648 (2020).
- [18] M. Xu, K. Yamamoto, J. Puebla, K. Baumgaertl, B. Rana, K. Miura, H. Takahashi, D. Grundler, S. Maekawa, and Y. Otani, Nonreciprocal surface acoustic wave propagation via magneto-rotation coupling, *Sci. Adv.* **6**, eabb1724 (2020).
- [19] M. Küß, M. Heigl, L. Flacke, A. Hörner, M. Weiler, M. Albrecht, and A. Wixforth, Nonreciprocal Dzyaloshinskii-Moriya Magnetoacoustic Waves, *Phys. Rev. Lett.* **125**, 217203 (2020).
- [20] R. Verba, E. N. Bankowski, T. J. Meitzler, V. Tiberkevich, and A. Slavin, Phase Nonreciprocity of Microwave-Frequency Surface Acoustic Waves in Hybrid Heterostructures with Magnetoelastic Coupling, *Adv. Electron. Mater.* **7**, 2100263 (2021).
- [21] Derek A. Bas, Piyush J. Shah, Michael E. McConney, and Michael R. Page, Optimization of acoustically-driven ferromagnetic resonance devices, *J. Appl. Phys.* **126**, 114501 (2019).
- [22] P. Grünberg, Magnetostatic spin-wave modes of a heterogeneous ferromagnetic double layer, *J. Appl. Phys.* **52**, 6824 (1981).
- [23] R. A. Gallardo, T. Schneider, A. K. Chaurasiya, A. Oelschlägel, S. S. P. K. Arekapudi, A. Roldán-Molina, R. Hübner, K. Lenz, A. Barman, J. Fassbender, *et al.*, Reconfigurable Spin-Wave Nonreciprocity Induced by Dipolar Interaction in a Coupled Ferromagnetic Bilayer, *Phys. Rev. Appl.* **12**, 034012 (2019).
- [24] M. Weiler, L. Dreher, C. Heeg, H. Huebl, R. Gross, M. S. Brandt, and S. T. B. Goennenwein, Elastically Driven Ferromagnetic Resonance in Nickel Thin Films, *Phys. Rev. Lett.* **106**, 117601 (2011).
- [25] A. S. Andrushchak, B. G. Mytsyk, H. P. Laba, O. V. Yurkevych, I. M. Solskii, A. V. Kityk, and B. Sahraoui, Complete sets of elastic constants and photoelastic coefficients of pure and MgO-doped lithium niobate crystals at room temperature, *J. Appl. Phys.* **106**, 073510 (2009).
- [26] K. Yamanouchi, in *Proceedings of the 1998 IEEE Ultrasonics Symposium (Cat. No. 98CH36102)*, Sendai, Japan, 1998, edited by S. C. Schneider, M. Levy, B. R. McAvoy (IEEE, New York, 1998), Vol. 1, pp. 57.
- [27] <https://www.pasternack.com/isolators-category.aspx>
- [28] R. Verba, V. Tiberkevich, and A. Slavin, Damping of linear spin-wave modes in magnetic nanostructures: Local, non-local, and coordinate-dependent damping, *Phys. Rev. B* **98**, 104408 (2018).
- [29] H. Matsumoto, T. Kawada, M. Ishibashi, M. Kawaguchi, and M. Hayashi, Large surface acoustic wave nonreciprocity in synthetic antiferromagnets, *Appl. Phys. Express* **15**, 063003 (2022).
- [30] J. Lou, R. E. Insignares, Z. Cai, K. S. Ziemer, M. Liu, and N. X. Sun, Soft magnetism, magnetostriction, and microwave properties of FeGaB thin films, *Appl. Phys. Lett.* **91**, 182504 (2007).